Antenna Radiation Pattern Measurements Using a Reverberation Chamber

Audrey K. Puls[12]
Dept. of Electrical, Computer, and Energy Engineering
University of Colorado – Boulder
Boulder, CO, USA
audrey.puls@colorado.edu

John M. Ladbury[3]
National Institute of Standards and Technology
Boulder, CO, USA
john.ladbury@nist.gov

William F. Young
University of Colorado – Denver
Denver, CO, USA
william.young@ucdenver.edu

Abstract— **This paper investigates the use of a reverberation chamber for antenna radiation pattern measurements allowing for significant cost reduction compared to anechoic environments. Our method utilizes averaging of paddle measurements to replicate anechoic data. We discuss both a correlation experiment, to determine how many degrees the reverberation paddle must rotate to create an uncorrelated measurement based on a 0.5 correlation threshold, and a radiation pattern measurement. Two matched horn antennas are used and operated between 1 GHz and 18 GHz. Good agreement is found between our measurements taken in a reverberation chamber and those taken by the manufacturer of the antenna in an anechoic chamber. We find that the main lobe radiation pattern of our antenna can be estimated with more certainty than the back-lobe radiation using a reverberation chamber. The goal is to use this simple and cost-effective method to determine radiation patterns for embedded antennas with unknown patterns, such as those within wireless devices.**

Keywords— Anechoic Chamber, Correlation, Directivity, Horn Antenna, Reverberation Chamber, Standard Deviation of the Mean, Vector Network Analyzer.

I. Introduction

Antenna radiation pattern measurements are typically performed in an anechoic chamber. These chambers are often expensive to install and inconvenient to rent from external facilities. Validating a lower cost method for these measurements is of general interest. Reverberation chambers are well understood [1] but have only recently been used for radiation pattern measurements [2][3] due to their significant cost reduction compared to anechoic environments. While [2] and [3] use plane wave decomposition, spherical wave decomposition, and Doppler effects to extract a radiation pattern, our approach lends simplicity to the problem by averaging scattering parameter data of uncorrelated paddle-positions. In this way, the variations in power, due to the position of the paddles, can be averaged out to mimic the isotropic environment typically found in an anechoic chamber. Our radiation pattern data will be shown and compared with manufacturer data taken in an anechoic chamber.

This method can potentially be used to measure radiation patterns of embedded antennas with unknown patterns, such as those within wireless devices.

The method discussed in this work utilizes an unloaded reverberation chamber, of dimensions 4.74 meters long by 4.13 meters wide by 5.18 meters tall, mode-stirring paddle, robotic arm, tripod, vector network analyzer, two horn antennas operating between 1 GHz and 18 GHz, and software to create an automated data collection system.

This paper is summarized as follows: Section II describes a paddle correlation experiment similar to that described in [4] and is performed to determine how many degrees the reverberation chamber paddle must rotate to create an uncorrelated measurement. This is important as it determines the minimum set of data, and hence shortest data collection time required to gather all necessary data. Section III uses the paddle step size correlation data from Section II to setup and determine the antenna radiation pattern measurements in a reverberation chamber. Section IV concludes this paper.

II. Reverberation Chamber Paddle Correlation

This section describes the reverberation chamber paddle-angle correlation experiment which determines how many degrees the vertical reverberation chamber paddle must rotate to produce an uncorrelated measurement. The chamber also contains a horizontal paddle, which is kept fixed during the experiment. In this way, we replicate a single stirrer reverberation chamber which is most commonly used and most likely to be procured by other facilities who may wish to reproduce this work.

A. Setup and Procedure

The setup for the paddle correlation experiment is shown in Fig. 1. The horizontal paddle is not shown as it is stationary for the duration of the test. The setup uses one horn antenna (our antenna under test (AUT)) attached to a robotic arm, which can rotate in the horizontal plane, and one horn

[1] This work was performed under the financial assistance award 70NANB18H006 from U.S. Department of Commerce, National Institute of Standards and Technology"

[2] Associate of the National Institute of Standards and Technology, Boulder, Colorado 80305, USA

antenna (our measurement antenna) attached to a stationary tripod. Both are connected to a vector network analyzer outside the chamber through bulkhead connections in the wall of the reverberation chamber. Note that the paddle is asymmetric about 180°. That is, if the paddle is rotated 1° clockwise, data will differ from that obtained when rotated 1° counterclockwise.

The antennas are cross-polarized and oriented with the main beams pointed away from each other in different height planes to minimize direct line-of-sight coupling and ensure coupling through reflections, thus aiding in creating a well-stirred environment.

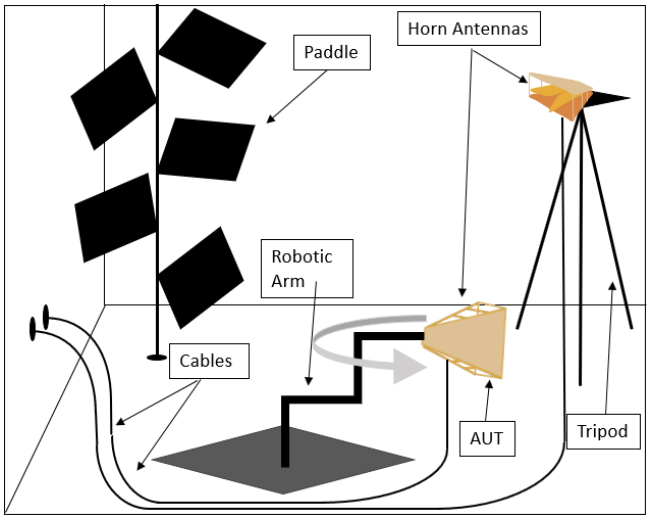

Fig. 1. Reverberation chamber paddle-angle correlation experiment setup. The antennas are cross polarized, in different height planes, and oriented away from each other to minimize direct line-of-sight coupling and ensure coupling through reflections in the chamber. Note that the arrow does not necessarily show the direction of rotation, but rather illustrates the axis of rotation and joint from which the robot pivots in the horizontal plane.

The procedure measures transmission S-parameter data (S_{21}) when the paddle is positioned at zero degrees. The data are taken in real and imaginary format. The paddle is then moved in 1° increments taking data each time, until one full rotation is complete (i.e., 1° steps in a 360° rotation). This 360° rotation and measurements are repeated 50 times.

B. Post Processing and Results

The measured S_{21} data were averaged over 50 trials, in which real and imaginary components were averaged separately, resulting in one complex average sample value per paddle position. A linear autocorrelation function, which utilizes the Fourier transform, is used with a 0.5 correlation threshold to determine how many degrees the paddle must rotate to produce an uncorrelated measurement. Note that a 0.5 correlation threshold is used to remain consistent with what was done in [4]. However, a 1/e threshold could also be used, which would produce an 8° rotation for an uncorrelated measurement. Results at 1 GHz and 18 GHz are shown in Fig. 2 via a solid and dotted line respectively. Mathematically, the autocorrelation function doubles the data, which can be seen in the spread about the 360° mark in Fig. 2. For this reason, Fig. 2 shows 720° on the x-axis, and the final rotation measurement required by the paddle to form an uncorrelated measurement is half the bandwidth at 360° which yields 6° at 1 GHz. These results determine paddle step size (6°) which will be used to collect antenna radiation pattern measurements discussed in Section III.

C. Differences with Similar Work

While there are many similarities between this experiment and [4], there are also a few significant differences. The first is that our work uses a different chamber than in [4] so any values obtained in [4] will differ. In addition [4] used a loaded chamber, but we use an unloaded chamber. Also important is that [4] used two paddles (vertical and horizontal) while in our experiment only one vertical paddle is rotated. Lastly, the data shown in [4] utilized a circular autocorrelation, which results in 360 points on the x-axis of the Fig. 2 equivalent plot shown in [4]. This method allowed for the full bandwidth of the spike to be used to determine an uncorrelated measurement. Our method utilizes a linear autocorrelation which results in 720 points on the x-axis of Fig. 2. This method allows for the half bandwidth of the spike to be used to determine an uncorrelated measurement. Either method is valid and will produce similar results.

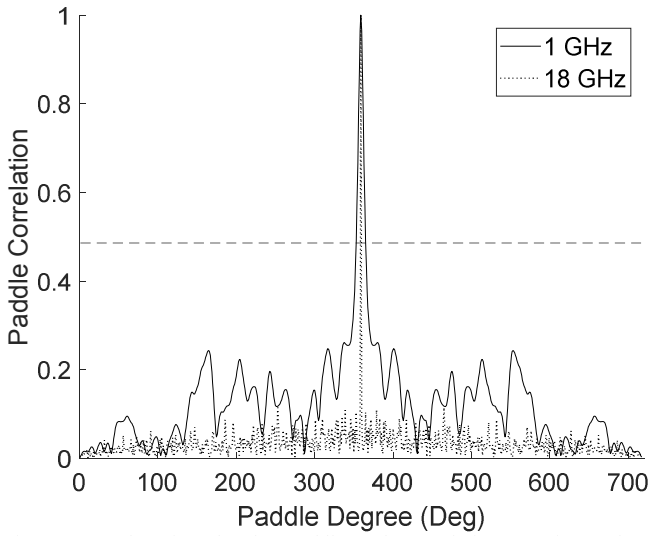

Fig. 2. Reverberation chamber paddle-angle correlation experiment data. Correlation results are indicated by half the bandwidth at 360° at the 0.5 correlation threshold mark. A 6° paddle rotation yields an uncorrelated measurement.

III. Antenna Radiation Pattern Measurements

This section will discuss the setup, procedure, and results of the antenna radiation pattern measurements in the reverberation chamber.

A. Setup and Procedure

The setup, shown in Fig. 3, aims to maximize transmission from one antenna to the other in order to collect the antenna radiation pattern. The idea is that the stirred energy will average to zero over the stirring sequence leaving only the line-of-sight, which corresponds to the antenna-to-

antenna coupling. For this reason, the antennas are co-polarized and directed at each other in the same height plane. Note also that the position of the tripod and attached antenna has changed from Fig. 1 to align the main lobe of the radiation pattern with the 0° mark, for easy comparison with manufacturer data, which will be shown later. Note that the antenna connected to the robot rotates in the horizontal plane.

The procedure starts by positioning the reverberation chamber paddles and both antennas at position zero (pointed towards each other) and collecting transmission data (S_{21}) in real and imaginary format. While both antennas are held constant, the vertical reverberation paddle is rotated in 6° increments until a full 360° rotation has been completed. This produces an uncorrelated measurement for frequencies between 1 GHz and 18 GHz using a 0.5 correlation threshold as found in the correlation study. Data are taken each time the paddle rotates 6°. The antenna attached to the robotic arm is then incremented by 1° and the process repeats until the antenna has made a full rotation.

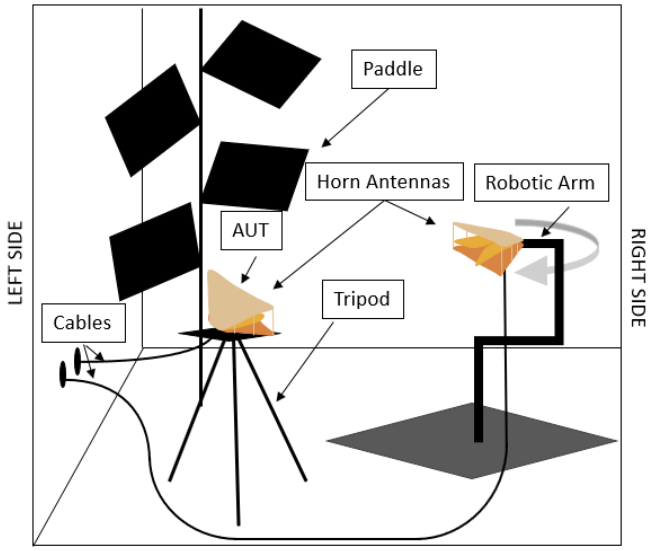

Fig. 3. Antenna pattern measurement setup in reverberation chamber. The antennas are co-polarized, pointed towards each other, and in the same height plane to maximize line-of-sight coupling. Note that the arrow does not necessarily show the direction of rotation, but rather illustrates the axis of rotation and joint from which the robot pivots in the horizontal plane.

Distances between the chamber and various components shown in Fig. 3 are given in Table I. Note that the antenna connected to the robot will rotate in the horizontal plane. Because of this, all measurements in Table I, that reference the antenna placed on the robot specify the position of the robot (towards the tripod antenna face or away from the tripod antenna face). The use of directional words (i.e., left and right) in Table I refer to the orientation specified in Fig. 3.

TABLE I. DISTANCES BETWEEN COMPONENTS IN FIG. 3 SETUP

Measurement Start	Measurement End	Value
Base of Tripod Antenna	Left Wall	75 cm
Tripod Antenna Face	Robot Antenna Face	61 cm
Base of Robot Antenna Pointed Towards Tripod Antenna	Right Wall	235 cm
Base of Robot Antenna Pointed 180° Away from Tripod Antenna	Right Wall	175 cm
Robot's Point of Rotation	Face of Robot Antenna	42 cm
Robot's Point of Rotation	Back Wall	235 cm
Robot's Point of Rotation	Front Wall	241 cm
Length of Chamber	N/A	4.74 m
Width of Chamber	N/A	4.13 m
Height of Chamber	N/A	5.18 m

B. *Post Processing and Results*

Plots showing the real and imaginary S_{21} components of the 60 paddle positions at 1, 3, 6, 12, and 18 GHz are shown in Fig. 4 when the antennas are pointed directly at each other. Note that the 60 paddle positions become more tightly grouped as the frequency increases, indicating lower uncertainties at higher frequencies. We will show that our radiation pattern data agree more closely with the radiation patterns measured by the manufacturer as the frequency increases.

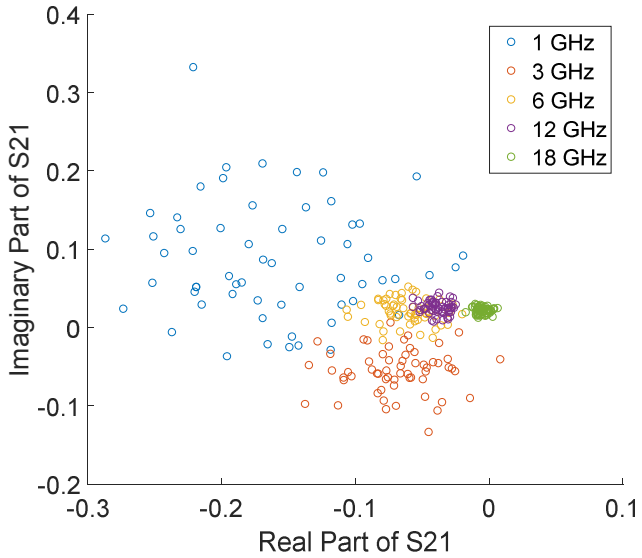

Fig. 4. 60 paddle positions at 1, 3, 6, 12, and 18 GHz when antennas are directly pointed at each other.

During post processing, all 60 paddle positions, taken each time the robotic arm antenna rotates 6°, are averaged (real and imaginary components are averaged separately). The magnitude of this complex value is taken and converted to dB. This value is what is plotted in Fig. 5 and Fig. 6. By averaging out the variations due to the paddle positions, the data mimics that which is typically taken in an anechoic

chamber. All data are frequency swept between 1 GHz and 18 GHz using 2001 equally-spaced points.

Radiation patterns in Fig. 5 and Fig. 6 show data from our measurements taken in a reverberation chamber compared with the manufacturer data taken in an anechoic chamber at 1, 3, 6, 12, and 18 GHz. No frequency averaging is performed on experimental data.

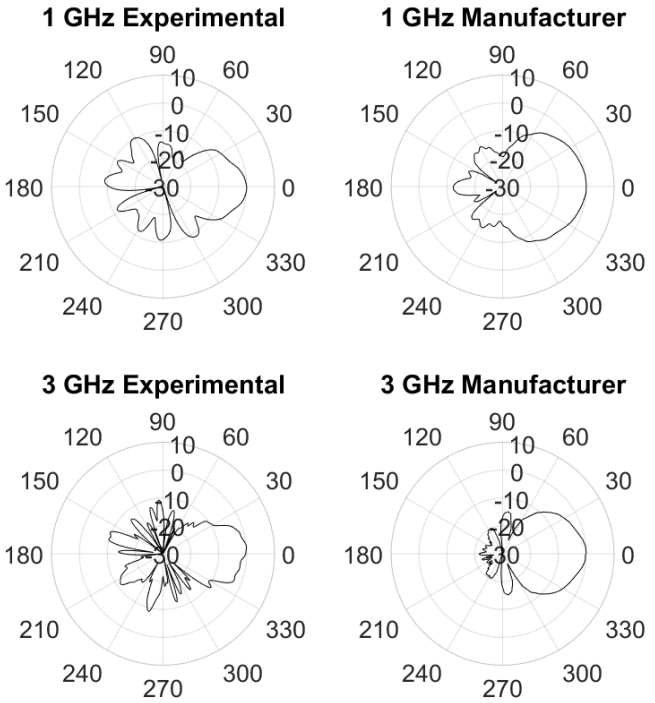

Fig. 5. Antenna-radiation pattern data from our experiment in the reverberation chamber (left) and from the manufacturer in an anechoic chamber (right) at 1 GHz and 3 GHz.

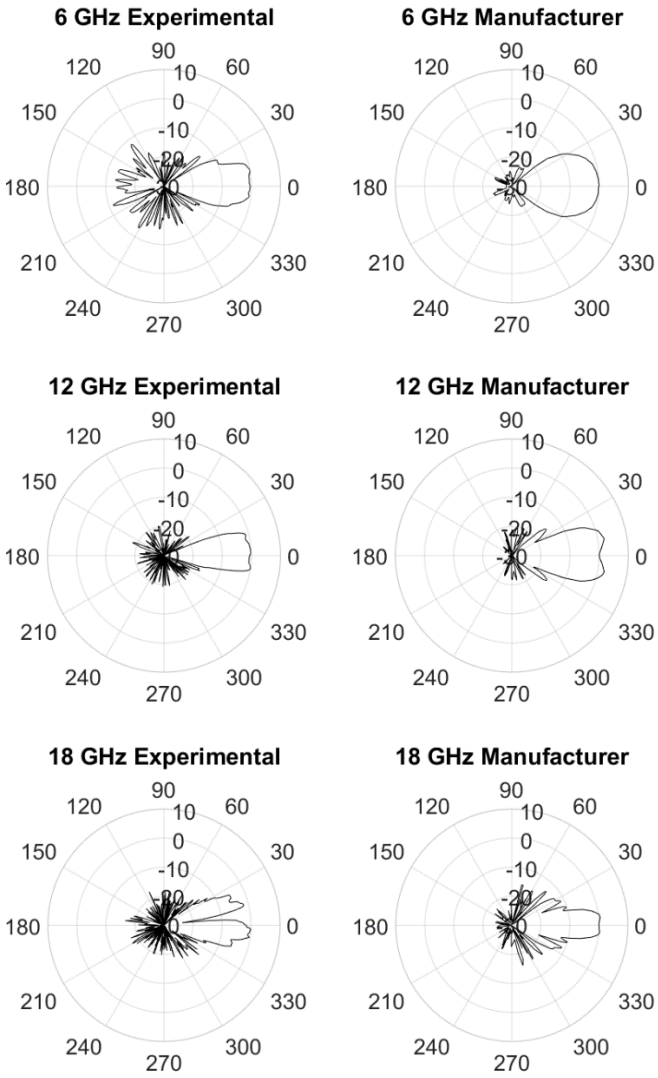

Fig. 6. Antenna-radiation pattern data from our experiment in the reverberation chamber (left) and from the manufacturer in an anechoic chamber (right) at 6 GHz, 12 GHz, and 18 GHz.

C. Estimate of Accuracy

The standard deviation of the mean (σ) gives an estimate of the variability of our data, and is calculated according to (1), where < > indicates complex averaging over all 60 paddle positions.

$$\sigma = \frac{\sqrt{<|S_{21}-<S_{21}>|^2>}}{\sqrt{N}}, \sqrt{N} = 60 \qquad (1)$$

If we divide $|<S_{21}>|$ by σ we can get an idea of the relative quality of the estimates at each frequency. This value would ideally be large, indicating σ is small relative to the measured $|<S_{21}>|$ value.

$|<S_{21}>|/\sigma$ ranges from 14 to 39 when the antennas are pointed at each other, and from 1 to 5 when one antenna is rotated 180 degrees away from the other for frequencies between 1 GHz and 18 GHz. The general trend of these values is to increase with frequency as the antennas align to

face each other. These data are plotted against frequency in Fig. 7.

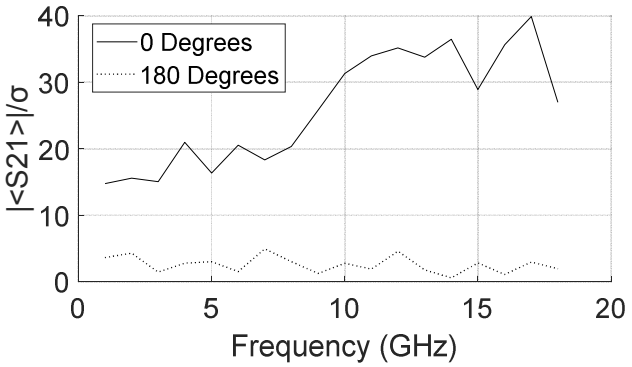

Fig. 7. $|<S_{21}>| / \sigma$ plotted against frequency when the faces of both antennas are pointed at each other (0° in legend, shown by solid line) and when the antenna connected to the robotic arm has rotated by 180° in the horizontal plane (180° in legend, shown by dotted line).

The estimate of quality decreases as the antenna connected to the robotic arm rotates further away from the face of the stationary antenna. This tells us that we are more confident in our ability to estimate the main lobe, and less confident in our sidelobe and back-lobe radiation estimate. This could explain why the experimental data of Fig. 5 and Fig. 6 show higher back-lobe radiation compared to manufacturer data.

Fig. 8 shows $|<S_{21}>|$ and σ versus frequency for antenna positions 0°, 5°, 20°, 90°, 180°, 270°, 340°, 355°, and 359°, where 0° indicates both antenna faces are pointed at each other, and 180° indicates the antenna on the robotic arm has been rotated by 180° in the horizontal plane. The ideal data would yield a σ that is significantly lower than $|<S_{21}>|$ in all cases. Fig. 8 shows that as the antenna connected to the robotic arm is rotated away from the face of the stationary antenna, σ and $|<S_{21}>|$ become closer together. This is a visual way of determining that our back-lobe radiation measurements are not as accurate as our main lobe measurements.

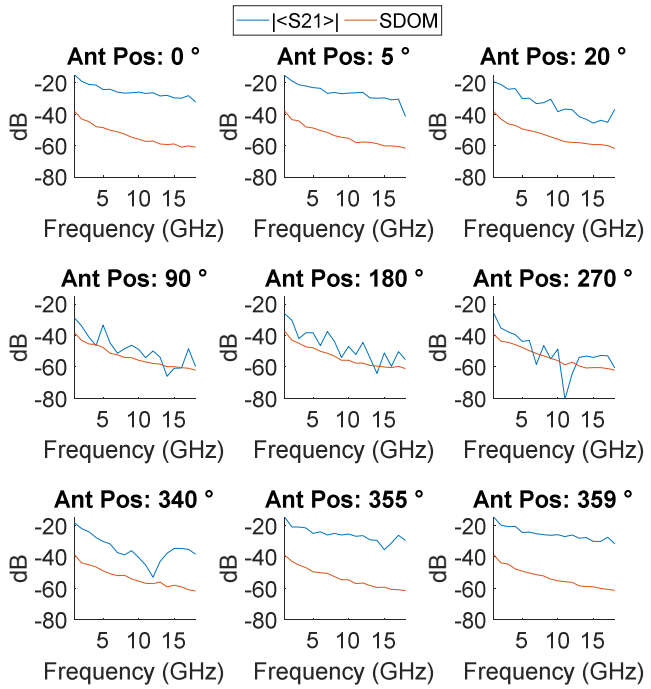

Fig. 8. S21 averaged over paddle positions and σ versus frequency for antenna positions 0°, 5°, 20°, 90°, 180°, 270°, 340°, 355°, and 359° where 0° indicates both antenna faces are pointed at each other, and 180° indicates one antenna has been rotated by 180° in the horizontal plane.

IV. Conclusion

The process described in this paper results in good agreement between experimental and manufacturer data, with high certainty in estimating the main lobe beams. Our certainty decreases as the antenna attached to the robotic arm rotates further from the stationary antenna face. Our data show enough certainty to demonstrate the potential of our simplistic and cost-effective method of antenna radiation pattern measurements in a reverberation chamber. In the future, radiation pattern measurements for the same horn antenna with the same experimental setup will be performed in our facilities' anechoic chamber to eliminate any experimental differences between the manufacturer anechoic chamber data and our experimental reverberation chamber data.

Acknowledgments

We acknowledge Jason Coder, Ryan Jacobs, Kate Remley, Robert Horansky, Robert Jones, and Michael Janezic for their help throughout this project.

References

[1] D. A. Hill, "Electromagnetic Theory of Reverberation Chambers," in National Institute of Standards and Technology NIST Tech. Note 1506, Boulder, CO, USA, Dec. 1998.

[2] M. Á. García-Fernández, D. Carsenat, and C. Decroze, "Antenna Radiation Pattern Measurements in Reverberation Chamber Using Plane Wave Decomposition," IEEE Trans. Antennas Propag., vol. 61, no. 10, pp. 5000–5007, Oct. 2013.

[3] Q. Xu, Y. Huang, "3D Antenna Radiation Pattern Reconstruction in a Reverberation Chamber Using Spherical Wave Decomposition," IEEE Trans. Antennas Propag., vol. 65, no. 4, pp. 1728-1739, Apr. 2017.

[4] Ryan J. Pirkl, Kate A. Remley, Christian S. Lötbäck Patané "Reverberation Chamber Measurement Correlation", IEEE Trans. Electromagnetic Compatibility, vol. 54, no 3, pp. 533-545, June 2012.